CHEMICAL PHYSICS

Time-optimized pulsed dynamic nuclear polarization

Kong Ooi Tan[1], Chen Yang[1], Ralph T. Weber[2], Guinevere Mathies[1]*, Robert G. Griffin[1†]

Pulsed dynamic nuclear polarization (DNP) techniques can accomplish electron-nuclear polarization transfer efficiently with an enhancement factor that is independent of the Zeeman field. However, they often require large Rabi frequencies and, therefore, high-power microwave irradiation. Here, we propose a new low-power DNP sequence for static samples that is composed of a train of microwave pulses of length τ_p spaced with delays *d*. A particularly robust DNP condition using a period $\tau_m = \tau_p + d$ set to ~1.25 times the Larmor period τ_{Larmor} is investigated which is a time-optimized pulsed DNP sequence (TOP-DNP). At 0.35 T, we obtained an enhancement of ~200 using TOP-DNP compared to ~172 with nuclear spin orientation via electron spin locking (NOVEL), a commonly used pulsed DNP sequence, while using only ~7% microwave power required for NOVEL. Experimental data and simulations at higher fields suggest a field-independent enhancement factor, as predicted by the effective Hamiltonian.

INTRODUCTION

Dynamic nuclear polarization (DNP) (*1*, *2*) is a powerful technique used to enhance the sensitivity of nuclear magnetic resonance (NMR) spectroscopy by transferring the high polarization of unpaired electrons to the nuclear spins of interest. The maximum enhancement factor is determined by the ratio of the electron to nuclear gyromagnetic ratios, which, for protons, is $\gamma_e/\gamma_{1H} \sim 658$. DNP experiments are typically performed by dispersing stable free radicals in a glassy matrix containing the sample of interest and by applying microwave irradiation at or near the electron Larmor frequency to mediate the polarization transfer. Over the past two decades, this technique, together with refinements in methods and instrumentation, has improved substantially particularly in magic angle spinning (MAS) NMR experiments conducted at high fields (>5 T) (*3*). However, essentially all current high-field DNP experiments use continuous-wave (CW) irradiation that exploits DNP mechanisms such as solid effect (SE), cross effect, or Overhauser effect (*4*–*8*). These DNP techniques have successfully enabled many new structural studies in both materials and biological science that were previously impossible, for instance, diamond nitrogen vacancy centers (*9*), membrane proteins (*10*, *11*), amyloid fibrils (*12*, *13*), and porous materials (*14*). However, the CW techniques have been predicted and demonstrated experimentally to yield a lower enhancement at higher fields. Accordingly, pulsed DNP techniques were proposed as promising and robust approaches to increasing sensitivity because the enhancement factor is theoretically field independent (*15*, *16*). Another advantage of using pulsed DNP methods is that the experiments can potentially be performed at higher temperatures for specific systems, rather than at cryogenic temperatures (<100 K), because the polarization transfer mechanism is not a saturation-based or CW technique. For instance, it was demonstrated experimentally that NOVEL (nuclear spin orientation via electron spin locking) was able to transfer polarization efficiently at room temperature (*15*, *17*). Despite a lower Boltzmann population, this could be an important advantage in situations where there is significant line broadening at lower temperatures.

Nevertheless, a concurrent disadvantage of the existing repertoire of pulsed DNP methods is that they often necessitate high microwave Rabi frequencies. For example, NOVEL (*15*, *18*, *19*) requires that the electron Rabi frequency, ω_{1S}, matches the nuclear Larmor frequency ω_{0I} ($\omega_{1S} = \omega_{0I}$) for optimal polarization transfer. This motivated us to search for different strategies to circumvent the direct dependence on the magnitude of the Rabi frequency, and we described two low-power alternatives, off-resonance NOVEL (*20*) and frequency-swept integrated SE (*21*, *22*). Both approaches yielded significant enhancements using only a fraction of microwave power required by NOVEL. In addition, a different pulsed DNP mechanism exploiting both electron paramagnetic resonance (EPR) and NMR excitation pulses combined with specific relaxation pathways was demonstrated on a special system of the endohedral fullerene, N@C60, although direct detection of the NMR signal was not reported (*23*). In this contribution, we demonstrate an alternate low-power approach where the DNP matching condition is predominantly determined by the strategic timing of the microwave pulses, rather than the Rabi fields. The experiment is inspired by the theory of dipolar recoupling experiments in MAS NMR.

In contemporary MAS NMR experiments, anisotropic interactions like dipolar couplings are attenuated by MAS yielding high-resolution spectra but are reintroduced during mixing periods to mediate polarization transfer. The reintroduction of dipolar couplings is known generically as recoupling (*24*, *25*), and they are often performed using rotor-synchronized pulse sequences such as radio frequency driven recoupling (RFDR) (*26*). In the case of DNP NMR, the pseudosecular hyperfine interaction is modulated by the larger nuclear Zeeman interaction in a mathematically similar way to the averaging of anisotropic interactions by MAS. Thus, we anticipate that the pseudosecular term can be recoupled to polarize the nuclei via microwave pulses time-synchronized with or close to the Larmor period. This is in analogy to rotor-synchronized sequences in MAS NMR. We show that by choosing the pulse length τ_p and delay *d* (Fig. 1) in a microwave pulse train strategically (*27*), i.e., satisfying the hyperfine recoupling condition (vide infra), an efficient and broad-banded DNP field profile can be achieved. In particular, we achieve enhancements ~15% larger than NOVEL but with only ~7% of the microwave power. Simulations performed for two cases at $\omega_{0I}/2\pi$ = 800 MHz suggest that efficient DNP can be performed at similarly modest Rabi frequencies. Accordingly, we denote such a sequence as TOP-DNP (time-optimized pulsed DNP).

[1]Francis Bitter Magnet Laboratory and Department of Chemistry, Massachusetts Institute of Technology, Cambridge, MA 02139, USA. [2]Bruker BioSpin Corporation, Billerica, MA 01821, USA.
*Present address: Department of Chemistry, University of Konstanz, 78464 Konstanz, Germany.
†Corresponding author. Email: rgg@mit.edu

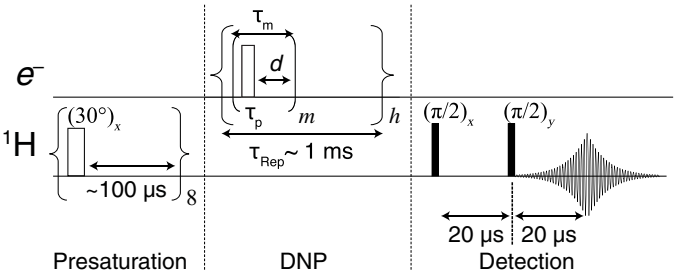

Fig. 1. Schematic diagram of a TOP-DNP sequence performed at 0.35 T. The TOP-DNP pulse sequence is composed of a train of *m* microwave pulses of a length τ_p separated by a delay *d* in between the pulses, in static (nonspinning) samples. The sequence is repeated *h* times with a repetition time τ_{Rep} to build up bulk ^{1}H polarization. The sequence becomes pulsed SE if $d = 0$.

Theory

We will show that the effective Hamiltonian of TOP-DNP can be derived analytically using Floquet theory (*28*–*33*). Let us consider a two-spin e^--^{1}H system with the general Hamiltonian in the electron rotating frame given by

$$\hat{\mathcal{H}}(t) = \Omega_S\hat{S}_z - \omega_{0I}\hat{I}_z + A\hat{S}_z\hat{I}_z + B\hat{S}_z\hat{I}_x + \omega_S(t)\hat{S}_x \quad (1)$$

The symbols *A* and *B* are the secular and nonsecular part of the hyperfine interaction, and the microwave Rabi field is $\omega_S(t) = \omega_{1S}$ during the pulse τ_p or $\omega_S(t) = 0$ during the delay *d* (Fig. 1). Next, an interaction-frame transformation is performed to obtain

$$\begin{aligned}\hat{\tilde{\mathcal{H}}}(t) &= \hat{U}_1^{-1}(t)\hat{U}_{0I}^{-1}\hat{\mathcal{H}}\hat{U}_{0I}\hat{U}_1(t) - (\Omega_S\hat{S}_z + \omega_S(t_1)\hat{S}_x - \omega_{0I}\hat{I}_z)\\ &= \hat{\tilde{S}}_z(t)\left(A\hat{I}_z + B(\hat{I}_x\cos(\omega_{0I}t) + \hat{I}_y\sin(\omega_{0I}t))\right) \quad (2)\end{aligned}$$

where $\hat{U}_1(t) = \hat{T}\exp(-i\int_0^t(\Omega_S\hat{S}_z + \omega_S(t_1)\hat{S}_x)dt_1)$, $\hat{U}_{0I}(t) = \exp(i\omega_{0I}t\hat{I}_z)$, $\hat{T}$ is the Dyson time-ordering operator, and

$$\begin{aligned}\hat{\tilde{S}}_z(t) &= \hat{U}_1^{-1}(t)\hat{S}_z\hat{U}_1(t) = \sum_{\chi=x,y,z} a_\chi(t)\hat{S}_\chi\\ &= \sum_{k=-\infty}^{\infty}\sum_{l=-1}^{1}\sum_{\chi=x,y,z} a_\chi^{(k,l)}e^{ik\omega_m t}e^{il\omega_{eff}t}\hat{S}_\chi \quad (3)\end{aligned}$$

Note that the time-dependent Hamiltonian $\hat{\tilde{\mathcal{H}}}(t)$ in the interaction frame (Eqs. 2 and 3) is modulated by the three characteristic frequencies (*29*, *30*) involved in TOP-DNP, namely, the nuclear Larmor frequency ω_{0I}, the modulation frequency $\omega_m = 2\pi/\tau_m$, and the effective field ω_{eff} (*29*, *30*). The modulation frequency is determined by the cycle time $\tau_m = \tau_p + d$ at which the sequence is repeated, and it is a fundamental parameter in designing pulse sequences for MAS NMR experiments. For instance, the value of τ_m is often chosen to be a multiple integer of the rotor period for a recoupling experiment, i.e., rotor-synchronized sequences. The effective field $\omega_{eff} = \beta_{eff}/\tau_m$ is defined as the net rotation angle β_{eff} over the cycle time τ_m of a periodic sequence. The notion of an effective or net rotation angle β_{eff} is an essential element in designing multiple-pulse sequences, and a feature that was exploited in a similar context when composite pulses were first introduced (*34*). A famous example includes the composite pulse ($90_y180_x90_y$) that generates an effective $\beta_{eff} = \pi$ pulse. If the composite pulse, or, in general, any multiple-pulse sequence, were to repeat itself periodically with a cycle time τ_m, then the Hamiltonian will be modulated by a frequency of $\omega_{eff} = \beta_{eff}/\tau_m$. Thus, the composite rotation induced by the pulse and a delay in TOP-DNP was determined using quaternions (*35*), and we obtained

$$\begin{aligned}\omega_{eff} &= 2\cos^{-1}(\cos(\Omega_S d/2)\cos(\omega_a\tau_p/2) -\\ &\cos\theta\sin(\Omega_S d/2)\sin(\omega_a\tau_p/2))/\tau_m \quad (4)\end{aligned}$$

where $\omega_a = \sqrt{{\omega_{1S}}^2 + {\Omega_S}^2}$ and $\theta = \tan^{-1}(\omega_{1S}/\Omega_S)$ (see the Supplementary Materials for derivation). Note that the effective field ω_{eff} has an indirect dependence on the Rabi ω_{1S} and offset $\Omega_S = \omega_e - \omega_{\mu w}$ frequencies. This could be advantageous because it relieves the critical dependence of the transfer efficiency on the Rabi frequency across the sample or pulse imperfections, as anticipated from the concept of composite pulse. Note that the sequence reduces to the SE ($\omega_{eff} = \omega_a$) in the special case of $d = 0$.

The effect of the characteristic frequencies ω_m and ω_{eff} in the interaction-frame Hamiltonian and information are embedded in the Fourier coefficients $a_\chi^{(k,l)}$ (Eq. 3), which are complex numbers bounded by $|a_\chi^{(k,l)}| \leq 1$. They can be interpreted as the scaling factors (*29*, *30*, *36*) that dictate the performance of a particular TOP-DNP sequence. For instance, a large scaling factor that scales the polarization transfer terms (vide infra) is desirable for robust performance. The coefficients $a_\chi^{(k,l)}$ were calculated numerically by Fourier-transforming the interaction-frame trajectory of the $\hat{S}_z(t)$ term (Eq. 3), i.e., $a_\chi^{(k,l)} = \int_0^T a_\chi(t)e^{-ik\omega_m t}e^{-il\omega_{eff}t}dt$. The integration limits in a Fourier transform are, by definition, from $-\infty$ to ∞. However, this is not computationally practical, and we have chosen a value for time *T*, such that it is longer than both $2\pi/\omega_{eff}$ and $2\pi/\omega_m$, to ensure the convergence on the value of $a_\chi^{(k,l)}$. Alternatively, the coefficients can be determined efficiently using a more advanced method introduced recently (*31*). The analytical description of the interaction-frame transformation and the calculation of the Fourier coefficients (Eq. 3) were performed in Mathematica (Wolfram Research) and MATLAB, respectively.

By combining Eqs. 2 and 3, we can rewrite $\hat{\tilde{\mathcal{H}}}(t)$ as a Fourier series with three characteristic frequencies

$$\hat{\tilde{\mathcal{H}}}(t) = \sum_{n=-1}^{1}\sum_{k=-\infty}^{\infty}\sum_{l=-1}^{1}\hat{\tilde{\mathcal{H}}}^{(n,k,l)}e^{in\omega_{0I}t}e^{ik\omega_m t}e^{il\omega_{eff}t} \quad (5)$$

with the Fourier components $\hat{\tilde{\mathcal{H}}}^{(n,k,l)}$ given by

$$\begin{aligned}\hat{\tilde{\mathcal{H}}}^{(0,k,l)} &= A\left(a_x^{(k,l)}\hat{S}_x + a_y^{(k,l)}\hat{S}_y + a_z^{(k,l)}\hat{S}_z\right)\hat{I}_z\\ \hat{\tilde{\mathcal{H}}}^{(\pm1,k,l)} &= \frac{B}{2}\left(a_x^{(k,l)}\hat{S}_x + a_y^{(k,l)}\hat{S}_y + a_z^{(k,l)}\hat{S}_z\right)(\hat{I}_x \mp i\hat{I}_y)\end{aligned} \quad (6)$$

Last, the first-order effective Hamiltonian, given by $\hat{\bar{H}}^{(1)} = \hat{\tilde{\mathcal{H}}}^{(0,0,0)} + \Sigma\hat{\tilde{\mathcal{H}}}^{(n,k,l)}$, can be determined if the matching conditions are fulfilled

$$n\omega_{0I} + k\omega_m + l\omega_{eff} = 0 \quad (7)$$

where n and l are integer numbers running from −1 to 1 and k is an integer. The absolute values of both n and l are limited to 1 because we consider only one proton in the system. In principle, they can be larger integers when more nuclei are involved and higher-order terms can appear. An alternate interpretation of the DNP matching condition (Eq. 7) is when the sum or difference of the time ratio τ_m/τ_{Larmor}, with the effective rotation $\beta_{eff}/2\pi$, is equal to an integer number k, i.e., $\tau_m/\tau_{Larmor} \pm \beta_{eff}/2\pi = k$. Again, the idea of matching the rotations induced by the microwave irradiation, the periodicity of the pulses, and the Larmor interaction to transfer polarization condition is anticipated from the recoupling experiments in MAS NMR. We will focus on $\hat{\tilde{\mathcal{H}}}^{(\pm1,k,l)}$ (Eq. 6) because $\hat{\tilde{\mathcal{H}}}^{(0,k,l)}$ commutes with the nuclear $\hat{I}_z$ terms and thus cannot mediate polarization transfer. Numerical simulations were performed (results not shown) to ensure that the presence of A in $\hat{\tilde{\mathcal{H}}}^{(0,0,0)}$ is insignificant and can be safely neglected.

There are, in principle, many ways of choosing the frequencies ω_{0I}, ω_m, and ω_{eff} to satisfy the hyperfine recoupling conditions (Eq. 7). Nevertheless, we will focus on the matching condition $\omega_m + \omega_{eff} = \omega_{0I}$, which results in the effective Hamiltonian given by

$$\hat{\tilde{\mathcal{H}}}^{(1,-1,-1)} + \hat{\tilde{\mathcal{H}}}^{(-1,1,1)} = \frac{B}{4}(a_-^{(-1,-1)}\hat{S}^-\hat{I}^- + a_+^{(-1,-1)}\hat{S}^+\hat{I}^- + 2a_z^{(-1,-1)}\hat{S}_z\hat{I}^-) + \text{c.c.} \quad (8)$$

and another matching condition $2\omega_m - \omega_{eff} = \omega_{0I}$ with effective Hamiltonian

$$\hat{\tilde{\mathcal{H}}}^{(1,-2,1)} + \hat{\tilde{\mathcal{H}}}^{(-1,2,-1)} = \frac{B}{4}(a_-^{(-2,1)}\hat{S}^-\hat{I}^- + a_+^{(-2,1)}\hat{S}^+\hat{I}^- + 2a_z^{(-2,1)}\hat{S}_z\hat{I}^-) + \text{c.c.} \quad (9)$$

The symbol c.c. stands for complex conjugate, $\hat{S}^{\pm} = \hat{S}_x \pm i\hat{S}_y$ are the ladder operators, and $a_{\pm}^{(k,l)} = a_x^{(k,l)} \mp i a_y^{(k,l)}$. The operators $\hat{S}^-\hat{I}^-$, $\hat{S}^+\hat{I}^-$, and $\hat{S}_z\hat{I}^-$ are double-quantum (DQ), zero-quantum (ZQ), and single-quantum (SQ) terms, respectively. The DQ and ZQ terms are responsible for mediating positive and negative polarization transfer, respectively, while the SQ terms could interfere with the transfer term if their magnitudes become comparable to the DQ/ZQ terms. In an ideal situation, a purely ZQ or DQ effective Hamiltonian is desired for an efficient polarization transfer. Thus, the difference between ZQ and DQ contributions, i.e., the magnitudes of a_- and a_+ coefficients in the effective Hamiltonian (Eq. 8), is computed to gauge the performance of TOP-DNP (vide infra).

RESULTS

Experimental and numerical results at 0.35 T

An EPR spectrum of trityl and DNP field profiles for pulsed SE (*20*) and NOVEL are shown in Fig. 2A. We obtained a maximum enhancement of $\varepsilon \sim 172$ at the NOVEL condition, $\omega_{1S}/(2\pi) \sim 15$ MHz (see the Supplementary Materials), and we recorded $\varepsilon \sim 150$ and -170 at the SE condition, $\Omega \pm \omega_{0I}$. Following that, we transformed the pulsed SE sequence into the TOP-DNP sequence by interleaving the microwave pulses of length τ_p with delays of duration d. We found a robust DNP condition using the parameters $\tau_m/\tau_{Larmor} \sim 1.25$ with $\tau_p = 28$ ns and

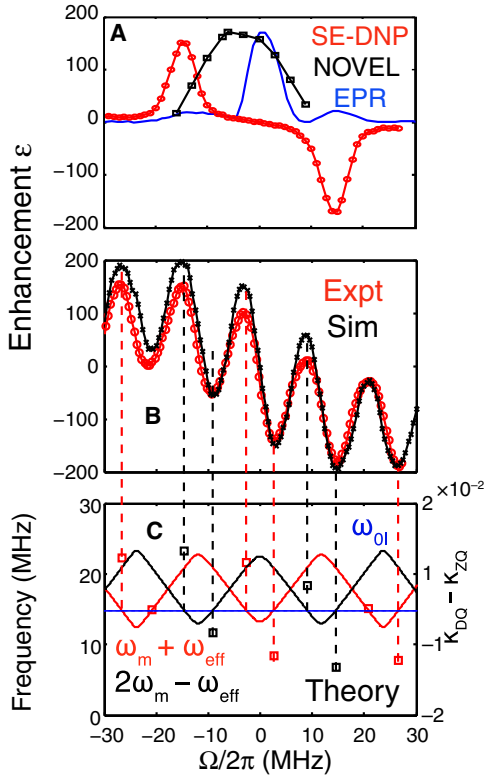

Fig. 2. EPR spectrum, field profiles of various DNP experiments, and calculated characteristic frequencies of TOP-DNP at 0.35 T. DNP enhancements of (**A**) pulsed SE and NOVEL, (**B**) TOP-DNP, and (**C**) the matching conditions as a function of $\Omega = \omega_{ELDOR} - \omega_e$. In (C), the matching conditions are fulfilled at the intersections between ω_{0I} (blue) and $\omega_m + \omega_{eff}$ (red) or $2\omega_m - \omega_{eff}$ (black), which can then be compared to the experimental (Expt)/simulated (Sim) results (B) via the vertical dashed lines. The values of the scaling factors $\kappa_{DQ} - \kappa_{ZQ}$ (square markers of respective colors) are shown on the right y axis.

$d = 56$ ns, which then yields a field profile (Fig. 2B) that is notably different from the one obtained with the SE. One can see that the TOP-DNP field profile has multiple DQ and ZQ DNP conditions spanning a very broad range of frequencies, i.e., at $\Omega \sim \pm 0.25\ \omega_{0I}, \pm\omega_{0I}$, and $\pm 2\omega_{0I}$. Using a Rabi frequency of $\omega_{1S}/(2\pi) = 4$ MHz at $\Omega/(2\pi) \sim 29$ MHz, we observed a maximum enhancement of ~200, which is higher than $\varepsilon \sim 172$ from NOVEL. The lower enhancement in NOVEL is likely because it is more susceptible to resonance mismatch, which explains superior improvement in adiabatic NOVEL (*37*).

In addition, we performed numerical simulations using a custom simulation package in MATLAB (The MathWorks) to substantiate the experimental results. We performed the simulations on a three-spin e^--^{1}H-^{1}H system. We found that the major features observed in the experimental data, i.e., the positions and the intensities of the DNP minima/maxima, are well reproduced in the numerical simulation on a three-spin system. Initial simulations using idealized parameters without relaxation yielded high enhancement factors that were larger than the experimental results. This is because each radical is, in reality, surrounded by many solvent protons. We have therefore incorporated a relaxation mechanism by introducing relaxation superoperators (*38*, *39*) in the Liouville space into the simulation package. We have adapted the values for the relaxation parameters, number of loops m, and h, so that the simulated enhancement resembles a more realistic value of ~200. The details of the simulation package and the values of

the parameters used for the experimental and simulated data are shown in Table 1.

In addition, we also calculated the characteristic frequencies $\omega_m + \omega_{eff} = \omega_{0I}$ and $2\omega_m - \omega_{eff} = \omega_{0I}$ (Eqs. 4 and 7) to verify the DNP matching conditions observed in Fig. 2B. One can see that all the DNP conditions observed have been predicted accurately by the theoretical calculations (Fig. 2C). Nevertheless, satisfying the matching conditions does not dictate the signs and efficiencies of the DNP enhancements. Thus, the difference between the ZQ and DQ contributions $\kappa_{DQ} - \kappa_{ZQ} = |a_{-}^{(k,l)}| - |a_{+}^{(k,l)}|$ (Eqs. 8 and 9) is computed to dictate the sign and performance of the polarization transfer. One can infer from the resulting plot (Fig. 2C) that the scaling factor $\kappa_{DQ} - \kappa_{ZQ}$ is large and negative at $\Omega/(2\pi) \sim 27$ MHz, leading to a ZQ transfer with a strong negative enhancement. The converse is also true; i.e., a small positive value of $\kappa_{DQ} - \kappa_{ZQ}$ at $\Omega/(2\pi) \sim 9$ MHz predicts a weak positive enhancement. It also follows that the absence of DNP enhancement at $\Omega/(2\pi) = \pm 21$ MHz can be explained by realizing that the ZQ and DQ terms have almost equal sizes and thus canceled each other's contributions, despite the fulfillment of the matching conditions. Most features observed in the simulated field profiles, for instance, the positions, relative magnitude, and signs of the DNP conditions, are well predicted by the theoretical evaluation of the resonance conditions (Eq. 7) and the Fourier coefficients (Eqs. 8 and 9). On the other hand, the maximum scaling factor of TOP-DNP at this experimental condition (~0.02) is low by comparison to NOVEL's. Hence, we anticipate that TOP-DNP will have a longer buildup time and therefore be more susceptible to lower T_{2e} relative to NOVEL. We have measured the enhancement buildup curve (Fig. 3) as a function of mixing time τ_{mix} by incrementing the loop *m* (Fig. 1). The single exponential fit yields a time constant of $\tau_{1mix} \sim 2.5$ μs, which is longer than the ~300 ns reported for NOVEL in the literature (*19*). Nevertheless, the bulk polarization time τ_{1DNP} is found to be ~8.4 s (Fig. 3B) compared to ~8 s for NOVEL (*19*). For practical DNP NMR experiments, the recycle delay is set to ~1.3 τ_{1DNP} for optimal sensitivity, while the mixing time τ_{mix} is

Table 1. Values of the parameters used for both the experimental and simulated results.

	SE-DNP (experimental; Fig. 2A)	TOP-DNP (experimental; Fig. 2B)	TOP-DNP (simulated; Fig. 2B)	TOP-DNP (experimental; Fig. 3)	2D (experimental; Fig. 4)	TOP-DNP (experimental; Fig. 5A)	TOP-DNP (simulated; Fig. 5B)
$\omega_{1S}/(2\pi)$ (MHz)	4	4	4	4	2	20	50* 200†
$\Omega/(2\pi)$ (MHz)	—	—	—	3	4	—	—
τ_p (ns)	1800	28	28	28	—	10	0.7
d (ns)	0	56	56	56	—	14	0.8
m	1	115	8	—	350	400	8192
h	8192	35,840	512	—	8192	409,600‡	262,144
B_0 field (T)	0.35	0.35	0.35	0.35	0.35	1.2	18.8

*Performed at 18.8 T and τ_{Rep} = 100 μs on BDPA with isotropic hyperfine couplings of 5.3 and 5.6 MHz and *g* values of [2.0032, 2.0033, 2.0034] to mimic a Gaussian EPR line.
†Performed at 18.8 T and τ_{Rep} = 100 μs on trityl with literature *g* values of [2.00258, 2.00319, 2.00319] and with isotropic hyperfine couplings set to 0.
‡Performed using τ_{Rep} = 130 μs.

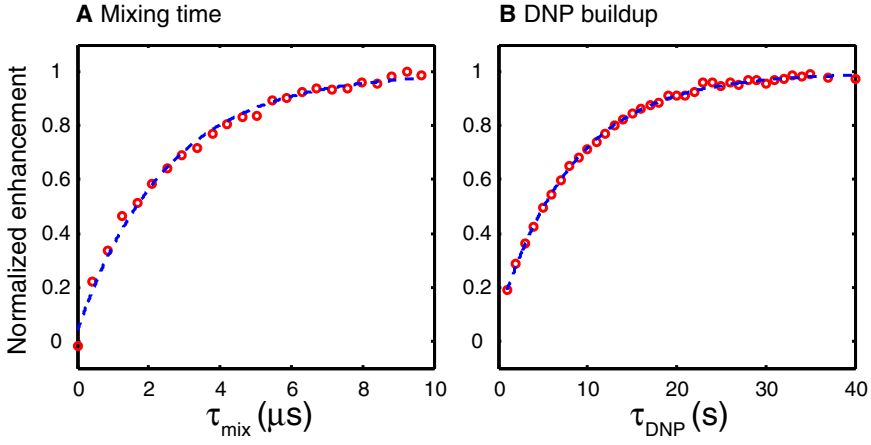

Fig. 3. Experimental buildup curves of TOP-DNP at 0.35 T. The buildup curves show the enhancement factor as a function of (**A**) the mixing time τ_{mix} by incrementing the loop *m*, which spans a period of $\tau_p + d$ = 84 ns, while keeping the time τ_{DNP} constant at ~8 s and (**B**) time τ_{DNP} by incrementing the loop *h* (Fig. 1) while keeping the time τ_{mix} constant at ~9.7 μs. The fitted single exponential curves (blue) yield time constants of (A) $\tau_{1mix} \sim 2.5$ μs and (B) $\tau_{1DNP} \sim 8.4$ s.

relevant only if the microwave amplifier has a limited operational duty cycle. Thus, we have demonstrated that the relatively low scaling factor of TOP-DNP has negligible influence on the performance of DNP NMR experiments.

To investigate the dependence of the matching conditions on the precise settings of the pulse width τ_p and delay d, we performed a pseudo–two-dimensional (2D) experiment to measure the DNP enhancement as a function of τ_p and d at a fixed offset Ω. The contour plot (Fig. 4) shows a narrow diagonal band of positive enhancement along the predicted condition $\omega_m - \omega_{eff} = \omega_{0I}$ and another broader diagonal band of negative enhancement at $\omega_m + \omega_{eff} = \omega_{0I}$. The experimental results show that the matching condition is sensitive to the cycle time $\tau_m = \tau_p + d$, much like the importance of ensuring rf pulses are synchronized with the rotor period during the recoupling sequences in MAS NMR experiments.

Experimental and numerical results at 1.2 and 18.8 T

It was shown that the effective Hamiltonians (Eqs. 8 and 9) do not have an explicit dependence on the static magnetic field B_0, as expected from the first-order recoupling sequence in MAS NMR. This opens the potential to theoretically attain large enhancement factors at higher fields, provided the timing of the microwave pulses and sufficiently high microwave power are feasible. Thus, we have investigated the sequence using the current state-of-the-art microwave amplifiers at ~1.2 T/34 GHz/51 MHz, which shows that an absolute enhancement of ~188 (Fig. 5A) was obtained using a Rabi frequency of $\omega_{1S}/(2\pi)$ = 20 MHz, τ_p = 10 ns, and d = 14 ns. The experimental result shows that a similar enhancement factor can be achieved upon repeating the TOP-DNP experiment at 1.2 T, which is a factor of ~3.5 times the magnetic field used in a previously shown experiment (Fig. 2A). This is a clear indication for a proof of principle that it is very likely that TOP-DNP will be as efficient at higher fields, as predicted theoretically.

Since the microwave technology to perform such an experiment at higher fields is under development (*40*, *41*), we performed a numerical simulation at 18.8 T using the matching condition $\tau_m/\tau_{Larmor} \sim 1.2$ (τ_p = 0.7 and d = 0.8 ns), as anticipated from scaling the parameters in our current experiment (τ_m = 84 ns at 0.35 T). The simulated field profile for trityl using $\omega_{1S}/2\pi$ = 200 MHz (Fig. 5B) yields an enhancement of ~200, which again demonstrates a field-invariant enhancement factor. In addition, we show that similar enhancement can be achieved on BDPA (1,3-bisdiphenylene-2-phenylallyl) using a lower Rabi field [$\omega_{1S}/(2\pi)$ = 50 MHz] because the radical is homogeneously broadened by ^{1}H hyperfine couplings and hence yields a narrower linewidth than trityl at high fields. The details of the parameters used for the numerical simulations are tabulated in Table 1. We note that these predicted power levels amount to <7% of that required to meet the NOVEL condition. Thus, TOP-DNP or a related sequence may well be the method of choice for DNP at very high fields.

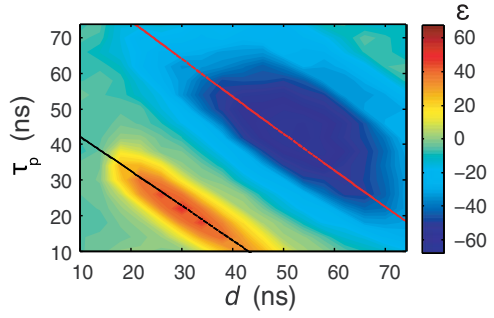

Fig. 4. A contour plot showing 2D optimization of the TOP-DNP enhancement factor against pulse length τ_p and delay d at 0.35 T. The experimental data were acquired using a Rabi frequency of $\omega_{1S}/(2\pi)$ = 2 MHz at a fixed offset of $\Omega/(2\pi)$ = 4 MHz, an optimum condition from the field profile (not shown). The matching conditions $\omega_m + \omega_{eff} = \omega_{0I}$ (red) and $\omega_m - \omega_{eff} = \omega_{0I}$ (black) are indicated with straight lines.

DISCUSSION

Inspired by recoupling sequences in MAS NMR, we proposed and examined a new hyperfine recoupling sequence, referred to as TOP-DNP, that is composed of a train of microwave pulses of a judiciously chosen width separated by delays. When the linear combination of the

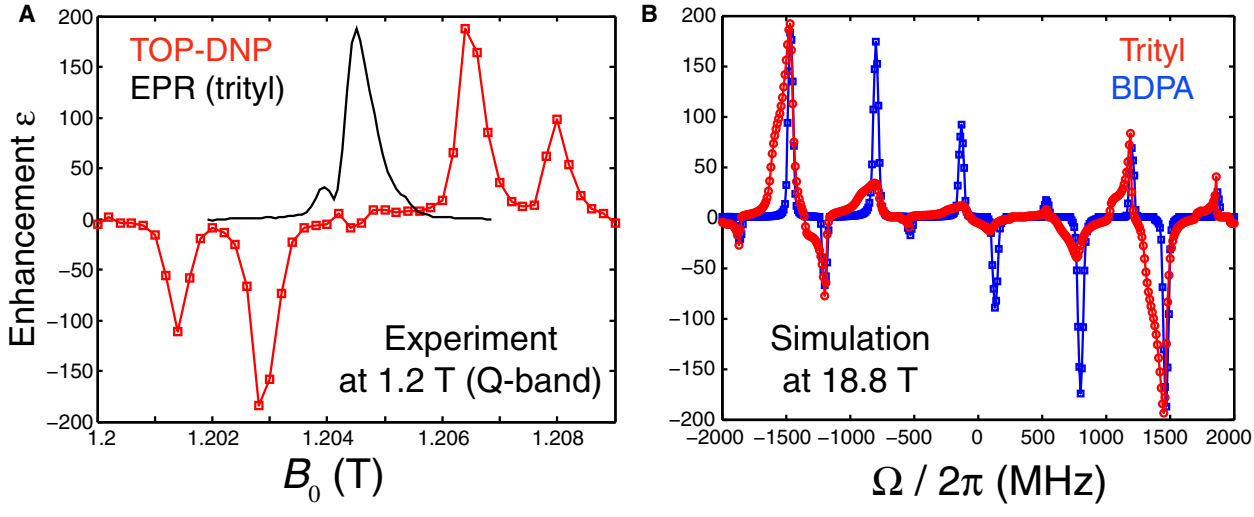

Fig. 5. TOP-DNP field profiles at 1.2 T (experimental) and 18.8 T (simulated). (**A**) The experiment was performed at ~1.2 T (Q-band) using a Rabi frequency of $\omega_{1S}/(2\pi)$ = 20 MHz, τ_p = 10 ns, and d = 14 ns. Note that the sign of enhancement appeared to be inverted compared to other field profiles because the data were acquired by varying the magnetic field B_0 while keeping the microwave frequency constant. (**B**) The simulated field profile at 18.8 T was performed using τ_p = 0.7 ns and d = 0.8 ns on trityl and BDPA with $\omega_{1S}/(2\pi)$ = 200 and 50 MHz, respectively. Further details are tabulated in Table 1.

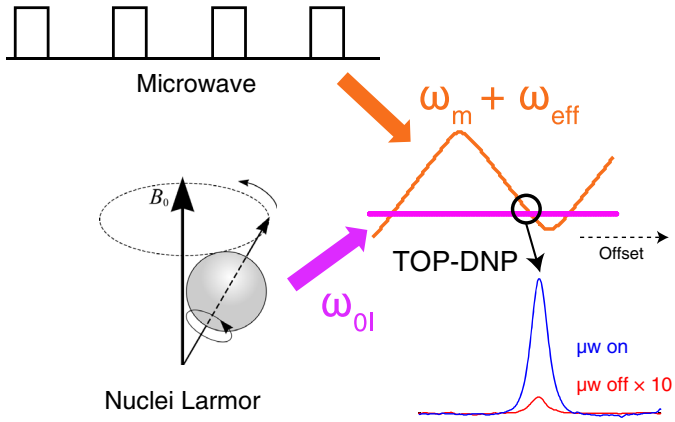

Fig. 6. Schematic diagram of the TOP-DNP experiment.

characteristic frequencies (ω_m and ω_{eff}) governed by the microwave pulse train matches the nuclei Larmor frequency (see Fig. 6), it results in the electron spin evolving with Fourier components at the nuclear Larmor frequency. This TOP-DNP effect then mediates transfer of polarization to the nuclei. The resulting field profile is multibanded and spans $4\omega_{0I}$ with a maximum ^{1}H enhancement of ~200 compared to $\varepsilon \sim 172$ for NOVEL at X-band frequencies. Moreover, a Rabi frequency of 4 MHz used in TOP-DNP represents ~7% of the microwave power needed for the case of NOVEL (~15 MHz at 0.35 T). This shows the utility of TOP-DNP over NOVEL at higher fields or microwave frequency, where high-power microwave sources are not readily available. Futhermore, numerical simulations and analytical theory are in good agreement with the experimental data. Last, experimental data at 1.2 T and numerical results at 18.8 T have confirmed that the enhancement of TOP-DNP is field independent, i.e., a promising candidate for DNP applications at higher fields. One of the issues expected of TOP-DNP at higher field is that it requires shorter pulse lengths and delays. These are technically feasible as commercial arbitrary waveform generators (for instance, M8190A, Keysight Technologies) have a time resolution of 11.1 ps. Moreover, a recent experiment demonstrated the capability of amplifying (*40*) ~100-ps pulses using a gyrotron amplifier (*41*). Alternatively, the issue can be circumvented using longer a pulse τ_p (or lower ω_m, which corresponds to a larger integer k in the matching condition; Eq. 7).

Another feature of the sequence is that its efficiency is primarily determined by the timing of the pulses and delays rather than the microwave power. This is advantageous because it is more reliable to control the timing than the microwave power, which can be inhomogeneous across the sample. Thus, we have demonstrated the innovative design of a pulsed DNP sequence by adopting a similar theoretical treatment in MAS NMR. We foresee that more advanced sequences involving phase modulation of microwave pulses can be investigated in future experiments, either for EPR, hyperfine recoupling (DNP), or decoupling (*42*).

MATERIALS AND METHODS

Experimental design at 0.35 T

We performed the experiments at 0.35 T/9.8 GHz/15 MHz on a sample of ~5 mM trityl OX063 in a mixture of d_8-glycerol/D_2O/H_2O (6:3:1 by volume), i.e., "DNP juice", at 80 K. All field profiles except NOVEL were obtained by varying the ELDOR (electron-electron double resonance) frequencies while keeping the magnetic field constant. The EPR spectrum was obtained by using spin echo detected spectra in a field-swept experiment at $\omega_{\mu w}/2\pi$ = 9.771 GHz. The presaturation of the ^{1}H channel (Fig. 1) was implemented before the DNP sequence to suppress the remaining NMR polarization. This is achieved using eight 30° pulses spaced by a delay (τ_{delay}) of 100 μs. An echo of the ^{1}H signal was generated using solid echo with τ_{SE} = 20 μs, so that the signal remains detectable beyond the receiver dead time and avoids the distortion by the ringdown in the probe. The ^{1}H spectrum at thermal equilibrium was measured with 1120 scans with a recycle delay of ~$3T_{1n}$ = 39 s. In this contribution, we define the enhancement factor as the signal measured scaled with the fully relaxed ^{1}H signal without microwave irradiation, calculated from the measured signal at ~$3T_{1n}$.

Experimental design at 1.2 T

We repeated the experiment at 1.2 T (Q-band) and at 80 K using the same sample, i.e., 5 mM trityl OX063 in "DNP juice", but loaded in a CFQ EPR tube with an outer diameter of 1.6 mm (Wilmad-LabGlass). The NMR acquisition was performed using a standard Bruker AVANCE II console with a 300-W rf amplifier connected to ENDOR probe model number Bruker EN5170-D2 via a Bruker H132224 tuning and matching circuit. In contrast to the NMR acquisition regime used at 0.35 T, we used spin echo ($\pi/2 - \tau - \pi - \tau -$ echo) with a delay of 40 μs, and $\pi/2$ and π pulse lengths of 4 and 8 μs, respectively, to attenuate the large ^{1}H background signal present in the probe. The residual ^{1}H contribution present in the DNP experiment was removed by taking a difference spectrum with and without a loaded sample tube. The relaxation times T_{1n} of the ^{1}H background and sample signals are ~1 and 40 s, respectively. Note that a relatively small loop number of m = 400 was used in TOP-DNP (Fig. 5A) due to a limitation of the EPR hardware. Consequently, a short repetition time (τ_{Rep})= of 130 μs was used to exploit the full duty cycle (~10%) of the 150 W microwave traveling-wave tube amplifier model Bruker E5805830.

Computational method

The DNP numerical simulations were performed in a Liouville space with powder orientations chosen using the Zaremba-Conroy-Cheng scheme (*43*). A point-dipole model was used to model both electron-nuclei dipolar couplings with a distance of 4.3 Å, and the isotropic hyperfine interaction was not considered, i.e., $a_{iso} = 0$. We used a set of g values = [2.0046, 2.0038, 2.0030] to mimic the EPR Gaussian signal in Fig. 2A. The Euler angles in the principal axis system for the g tensor and the hyperfine interactions for $e - n_1$ and $e - n_2$ are set to be (0°, 40°, 0°), (0°, 0°, 0°), and (30°, 90°, 70°), respectively. The relaxation mechanism was modeled using relaxation superoperators or double commutators $\hat{\Gamma} = \sum_{\chi=x,y,z} k_\chi \left[\hat{S}_\chi\left[\hat{S}_\chi, \sigma\right]\right]$ (*38*), where σ is the density operator and k_χ incorporates the details of the relaxation constants. The double commutator mimics the isotropic uncorrelated fluctuation of the local magnetic field that induces relaxations on the spin system. We used relaxation times of T_{1e} = 1 ms, T_{2e} = 5 μs and T_{1n} = 13 s, T_{2n} = 1 ms for the electron and ^{1}H nuclei, respectively. The details of the numerical simulation package will be discussed in a future publication.

SUPPLEMENTARY MATERIALS

Supplementary material for this article is available at http://advances.sciencemag.org/cgi/content/full/5/1/eaav6909/DC1

Section S1. Determining the effective field ω_{eff} with quaternions

Section S2. Experimental details of NOVEL

Fig. S1. Experimentally measured enhancements of the NOVEL sequence as a function of the Rabi frequency at 0.35 T.

REFERENCES AND NOTES

1. A. Abragam, M. Goldman, Principles of dynamic nuclear polarisation. *Rep. Prog. Phys.* **41**, 395–467 (1978).
2. T. R. Carver, C. P. Slichter, Polarization of nuclear spins in metals. *Phys. Rev.* **92**, 212–213 (1953).
3. L. R. Becerra, G. J. Gerfen, R. J. Temkin, D. J. Singel, R. G. Griffin, Dynamic nuclear polarization with a cyclotron resonance maser at 5 T. *Phys. Rev. Lett.* (1993).
4. A. Abragam, W. G. Proctor, Une nouvelle methode de polarisation dynamique des noyaux atomiques dans les solides. *Comp. Rend. Acad. Sci.* **246**, 2253–2256 (1958).
5. A. W. Overhauser, Polarization of nuclei in metals. *Phys. Rev.* **92**, 411–415 (1953).
6. C. F. Hwang, D. A. Hill, New effect in dynamic polarization. *Phys. Rev. Lett.* **18**, 110–112 (1967).
7. C. F. Hwang, D. A. Hill, Phenomenological model for the new effect in dynamic polarization. *Phys. Rev. Lett.* **19**, 1011–1014 (1967).
8. M. Borghini, Spin-temperature model of nuclear dynamic polarization using free radicals. *Phys. Rev. Lett.* **20**, 419–421 (1968).
9. I. Schwartz, J. Scheuer, B. Tratzmiller, S. Müller, Q. Chen, I. Dhand, Z.-Y. Wang, C. Müller, B. Naydenov, F. Jelezko, M. B. Plenio, Robust optical polarization of nuclear spin baths using Hamiltonian engineering of nitrogen-vacancy center quantum dynamics. *Sci. Adv.* **4**, eaat8978 (2018).
10. V. S. Bajaj, M. L. Mak-Jurkauskas, M. Belenky, J. Herzfeld, R. G. Griffin, Functional and shunt states of bacteriorhodopsin resolved by 250 GHz dynamic nuclear polarization–enhanced solid-state NMR. *Proc. Natl. Acad. Sci. U.S.A.* **106**, 9244–9249 (2009).
11. E. Lehnert, J. Mao, A. R. Mehdipour, G. Hummer, R. Abele, C. Glaubitz, R. Tampé, Antigenic peptide recognition on the human ABC transporter TAP resolved by DNP-enhanced solid-state NMR spectroscopy. *J. Am. Chem. Soc.* **138**, 13967–13974 (2016).
12. M. J. Bayro, G. T. Debelouchina, M. T. Eddy, N. R. Birkett, C. E. MacPhee, M. Rosay, W. E. Maas, C. M. Dobson, R. G. Griffin, Intermolecular structure determination of amyloid fibrils with magic-angle spinning and dynamic nuclear polarization NMR. *J. Am. Chem. Soc.* **133**, 13967–13974 (2011).
13. G. T. Debelouchina, M. J. Bayro, A. W. Fitzpatrick, V. Ladizhansky, M. T. Colvin, M. A. Caporini, C. P. Jaroniec, V. S. Bajaj, M. Rosay, C. E. Macphee, M. Vendruscolo, W. E. Maas, C. M. Dobson, R. G. Griffin, Higher order amyloid fibril structure by MAS NMR and DNP spectroscopy. *J. Am. Chem. Soc.* **135**, 19237–19247 (2013).
14. A. J. Rossini, A. Zagdoun, M. Lelli, A. Lesage, C. Copéret, L. Emsley, Dynamic nuclear polarization surface enhanced NMR spectroscopy. *Acc. Chem. Res.* **46**, 1942–1951 (2013).
15. T. V. Can, J. J. Walish, T. M. Swager, R. G. Griffin, Time domain DNP with the NOVEL sequence. *J. Chem. Phys.* **143**, 054201 (2015).
16. T. Maly, G. T. Debelouchina, V. S. Bajaj, K.-N. Hu, C.-G. Joo, M. L. Mak-Jurkauskas, J. R. Sirigiri, P. C. van der Wel, J. Herzfeld, R. J. Temkin, Dynamic nuclear polarization at high magnetic fields. *J. Chem. Phys.* **128**, 052211 (2008).
17. K. Tateishi, M. Negoro, S. Nishida, A. Kagawa, Y. Morita, M. Kitagawa, Room temperature hyperpolarization of nuclear spins in bulk. *Proc. Natl. Acad. Sci. U.S.A.* **111**, 7527–7530 (2014).
18. A. Henstra, P. Dirksen, J. Schmidt, W. T. Wenckebach, Nuclear spin orientation via electron spin locking (NOVEL). *J. Magn. Reson.* **77**, 389–393 (1988).
19. G. Mathies, S. Jain, M. Reese, R. G. Griffin, Pulsed dynamic nuclear polarization with trityl radicals. *J. Phys. Chem. Lett.* **7**, 111–116 (2016).
20. S. K. Jain, G. Mathies, R. G. Griffin, Off-resonance NOVEL. *J. Chem. Phys.* **147**, 164201 (2017).
21. T. V. Can, R. T. Weber, J. J. Walish, T. M. Swager, R. G. Griffin, Frequency-swept integrated solid effect. *Angew. Chem., Int. Ed.* **56**, 6744–6748 (2017).
22. T. V. Can, J. E. McKay, R. T. Weber, C. Yang, T. Dubroca, J. van Tol, S. Hill, R. G. Griffin, Frequency-swept integrated and stretched solid effect dynamic nuclear polarization. *J. Phys. Chem. Lett.* **9**, 3187–3192 (2018).
23. G. W. Morley, J. van Tol, A. Ardavan, K. Porfyrakis, J. Zhang, G. A. Briggs, Efficient dynamic nuclear polarization at high magnetic fields. *Phys. Rev. Lett.* **98**, 220501 (2007).
24. N. C. Nielsen, L. A. Strassø, A. B. Nielsen, Dipolar recoupling. *Top. Curr. Chem.* **306**, 1–45 (2012).
25. R. G. Griffin, Dipolar recoupling in MAS spectra of biological solids. *Nat. Struct. Biol.* **5**, 508–512 (1998).
26. A. E. Bennett, R. G. Griffin, J. H. Ok, S. Vega, Chemical shift correlation spectroscopy in rotating solids: Radio frequency-driven dipolar recoupling and longitudinal exchange. *J. Chem. Phys.* **96**, 8624 (1992).
27. G. Bodenhausen, R. Freeman, G. A. Morris, A simple pulse sequence for selective excitation in Fourier-transform NMR. *J. Magn. Reson.* **23**, 171–175 (1976).
28. I. Scholz, J. D. van Beek, M. Ernst, Operator-based floquet theory in solid-state NMR. *Solid State Nucl. Magn. Reson.* **37**, 39–59 (2010).
29. K. O. Tan, M. Rajeswari, P. K. Madhu, M. Ernst, Asynchronous symmetry-based sequences for homonuclear dipolar recoupling in solid-state nuclear magnetic resonance. *J. Chem. Phys.* **142**, 065101 (2015).
30. K. O. Tan, V. Agarwal, B. H. Meier, M. A. Ernst, Generalized theoretical framework for the description of spin decoupling in solid-state MAS NMR: Offset effect on decoupling performance. *J. Chem. Phys.* **145**, 094201 (2016).
31. R. Shankar, M. Ernst, P. K. Madhu, T. Vosegaard, N. C. Nielsen, A. B. Nielsen, A general theoretical description of the influence of isotropic chemical shift in dipolar recoupling experiments for solid-state NMR. *J. Chem. Phys.* **146**, 134105 (2017).
32. J. H. Shirley, Solution of the Schrödinger equation with a Hamiltonian periodic in time. *Phys. Rev.* **138**, B979–B987 (1965).
33. M. Leskes, P. K. Madhu, S. Vega, Floquet theory in solid-state nuclear magnetic resonance. *Prog. Nucl. Magn. Reson. Spectrosc.* **57**, 345–380 (2010).
34. M. H. Levitt, Composite pulses. *Prog. Nucl. Magn. Reson. Spectrosc.* **18**, 61–122 (1986).
35. B. Blümich, H. W. Spiess, Quaternions as a practical tool for the evaluation of composite rotations. *J. Magn. Reson.* **61**, 356–362 (1985).
36. M. H. Levitt, Symmetry-based pulse sequences in magic-angle spinning solid-state NMR. *Encycl. Nucl. Magn. Reson.* **9**, 165–196 (2007).
37. T. V. Can, R. T. Weber, J. J. Walish, T. M. Swager, R. G. Griffin, Ramped-amplitude NOVEL. *J. Chem. Phys.* **146**, 154204 (2017).
38. A. Karabanov, G. Kwiatkowski, W. Köckenberger, Spin dynamic simulations of solid effect DNP: The role of the relaxation superoperator. *Mol. Phys.* **112**, 1838–1854 (2014).
39. M. H. Levitt, L. Di Bari, Steady state in magnetic resonance pulse experiments. *Phys. Rev. Lett.* **69**, 3124–3127 (1992).
40. E. A. Nanni, S. Jawla, S. M. Lewis, M. A. Shapiro, R. J. Temkin, Photonic-band-gap gyrotron amplifier with picosecond pulses. *Appl. Phys. Lett.* **111**, 233504 (2017).
41. E. A. Nanni, S. M. Lewis, M. A. Shapiro, R. G. Griffin, R. J. Temkin, Photonic-band-gap traveling-wave gyrotron amplifier. *Phys. Rev. Lett.* **111**, 235101 (2013).
42. E. P. Saliba, E. L. Sesti, F. J. Scott, B. J. Albert, E. J. Choi, N. Alaniva, C. Gao, A. B. Barnes, Electron decoupling with dynamic nuclear polarization in rotating solids. *J. Am. Chem. Soc.* **139**, 6310–6313 (2017).
43. V. B. Cheng, H. H. Suzukawa, M. Wolfsberg, Investigations of a nonrandom numerical method for multidimensional integration. *J. Chem. Phys.* **59**, 3992 (1973).

Acknowledgments: We thank M. Ernst, A. B. Nielsen, and S. Jain for support and stimulating discussions. **Funding:** K.O.T. was supported by an Early Postdoc Mobility grant from the Swiss National Science Foundation (grant no. 165285). G.M. was supported by the Deutsche Forschungsgemeinschaft through an Emmy Noether Grant (project no. 321027114). The research was supported by grants to R.G.G. from the National Institutes of Biomedical Imaging and Bioengineering (EB-002804 and EB-002026). **Author contributions:** K.O.T. and R.G.G. designed and performed experiments, with assistance from G.M. and R.T.W. K.O.T. carried out the theoretical analysis. K.O.T. and C.Y. ran numerical simulations. K.O.T., C.Y., R.T.W., G.M., and R.G.G. wrote the paper. **Competing interests:** The authors declare that they have no competing interests. **Data and materials availability:** All data needed to evaluate the conclusions in the paper are present in the paper and/or the Supplementary Materials. Additional data related to this paper may be requested from the authors.

Submitted 11 October 2018
Accepted 5 December 2018
Published 18 January 2019
10.1126/sciadv.aav6909

Citation: K. O. Tan, C. Yang, R. T. Weber, G. Mathies, R. G. Griffin, Time-optimized pulsed dynamic nuclear polarization. *Sci. Adv.* **5**, eaav6909 (2019).

Time-optimized pulsed dynamic nuclear polarization

Kong Ooi Tan, Chen Yang, Ralph T. Weber, Guinevere Mathies and Robert G. Griffin

Sci Adv **5** (1), eaav6909.
DOI: 10.1126/sciadv.aav6909